Available online at www.sciencedirect.com
SCIENCE DIRECT®
Journal of Nuclear Materials 322 (2003) 80–86
journal of nuclear materials
www.elsevier.com/locate/jnucmat

In situ investigation of U(IV)-oxide surface dissolution and remineralization by electrochemical AFM

J. Römer [a], M. Plaschke [a,*], G. Beuchle [b], J.I. Kim [a]

[a] Forschungszentrum Karlsruhe, Institut für Nukleare Entsorgung, Postfach 3640, D-76021 Karlsruhe, Germany
[b] Forschungszentrum Karlsruhe, Institut für Technische Chemie, Postfach 3640, D-76021 Karlsruhe, Germany

Received 26 March 2003; accepted 3 July 2003

Abstract

Surface chemical processes of UO_2 are investigated on a nanoscopic scale by electrochemical atomic force microscopy (ECAFM) using a home-developed electrochemical cell. Dissolution reactions of the solid surface and subsequent remineralization are observed at the solid–water interface under different redox conditions and carbonate concentrations. The local dissolution rates vary between different grain faces, grain boundaries and etch pits. A correlation between dissolution rates and the grain orientations relative to the specimen surface can be demonstrated by electron backscatter diffraction (EBSD). Remineralization under oxidizing conditions occurs mainly at grain faces with higher dissolution rates. The remineralized products are particles of 200–900 nm in diameter and exhibit a tabular morphology. Profound knowledge of the UO_2 surface chemistry on a nanoscale may help to clarify the related mechanisms explaining the macroscopically observed dissolution rates.

1. Introduction

The release of radionuclides from spent fuel after an assumed contact with groundwater has to be considered for a safety assessment of a nuclear waste repository. The major part of radionuclides, i.e. actinides, is retained in the grains of sintered UO_2 pellets and will not be mobilized before the solid matrix dissolves. The UO_2 dissolution depends on physico-chemical parameters, such as pH, redox potential, carbonate concentration and the availability of oxidative radiolysis products [1]. An increasing dissolution rate is observed under oxidizing conditions because the solubility is higher for U(VI) than for U(IV). In addition, carbonate enhances the dissolution rate due to the complexation with the uranyl ion. The plausible mechanisms explaining the macroscopically observed dissolution rates are discussed in the literature [1,2]. Even though generally reducing conditions can be expected in a nuclear waste repository, the UO_2 surfaces are subject to an oxidizing environment over a long period of time due to the alpha radiolysis of water. While gamma radiolysis decreases markedly after about 500 years, alpha and beta radiolysis remain over periods of about 10^5 years. This period is beyond the life time of canister materials [3,4].

Electrochemical methods allow the adjustment of redox potentials which are considered to be relevant for surface chemical processes of the fuel matrix under waste disposal conditions [5,6]. By a combination with atomic force microscopy (AFM) (so-called electrochemical AFM, ECAFM) local dissolution rates can be quantified at the solid–liquid interface under the (electro-)chemical conditions of interest. In previous work ECAFM was mainly applied for the investigation of

* Corresponding author. Tel.: +49-7247 824747; fax: +49-7247 823927.
E-mail addresses: plaschke@ine.fzk.de, markus.plaschke@ine.fzk.de (M. Plaschke).

0022-3115/$ - see front matter © 2003 Elsevier B.V. All rights reserved.
doi:10.1016/S0022-3115(03)00319-2

corrosion processes of metals, such as steel, copper or titanium [7–10]. The atomic structure of UO_{2+x} in the presence of oxygen was studied by scanning tunneling microscopy in ultra-high vacuum and at elevated temperature [11]. In situ corrosion studies of the UO_2 surface applying ECAFM have not been published so far.

Electron backscatter diffraction (EBSD) introduced by Kikuchi is a technique for the determination of crystal orientations and phase identification in composite materials. High-energy electrons are scattered by the atomic planes of a crystalline sample. The diffraction pattern, the so-called Kikuchi or electron backscatter pattern, results from the interaction of elastically scattered electrons (acting as a point source) and the crystal planes. When electron waves originating from a point source constructively interfere with the grating of the crystal planes according to Bragg's law, a pattern is obtained with dimensions directly related to the grating. Considering the Bragg equation the interplanar spacings and angles of the most prominent lattice planes can be indexed and the crystal orientation can be calculated. Details of generation and processing of Kikuchi patterns and their application in texture analysis of metals and other materials are described in the literature [12,13].

As corrosion generally begins and proceeds at the fuel–water interface, the understanding of UO_2 surface chemistry is of high importance. Using ECAFM the composition of the aqueous environment and the redox potential can be varied and, thus, waste disposal conditions can be simulated. Their influence on surface chemical processes is studied in situ with a nanometer resolution. By combination with EBSD performed in an environmental scanning electron microscope (ESEM) the role of crystal orientation on matrix dissolution is examined.

2. Experimental

A sintered pellet of uranium dioxide (Joint Research Centre, Central Bureau for Nuclear Measurements (CBNM), Geel, Belgium) is used as sample which is characterized as a certified nuclear reference material (CBNM Reference Material No. 106). The uranium has an isotopic composition obtained by mass spectrometry of ^{238}U:99.2787, ^{235}U:0.7158, ^{234}U:0.0055 weight percent.

A commercial AFM (Topometrix, TMX 2000, Explorer) with a home-developed electrochemical cell is used (Fig. 1). The UO_2 sample is embedded in an epoxy resin using a holder of stainless steel and electrically contacted (working electrode). Additionally, flexible silicon tubes are embedded and used for the liquid exchange and salt bridge. This liquid cell enables the

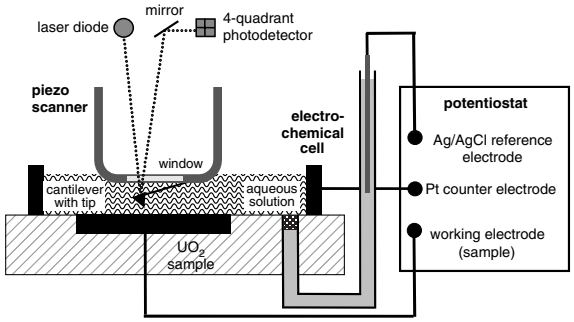

Fig. 1. Experimental setup of ECAFM (see Section 2).

preparation of a plane and fresh sample surface for several times by polishing. The counter electrode is a platinum coated ring of titanium which forms the wall of the liquid cell. The Ag/AgCl reference electrode (1 M KCl) is connected with an embedded tube and sealed with a ceramic diaphragma against the cell. At room temperature, the reference electrode has a potential of +236 mV against SHE (standard hydrogen electrode) [14]. $NaHCO_3$ solutions (3% or 0.3%) are adjusted to $pH = 8.7$ and filled in the liquid cell. The potential is adjusted by a bipotentiostate (type MP81, Bank Elektronik, Clausthal-Zellerfeld, Germany) to values ranging from −1.0 V (reducing) to +1.0 V (oxidizing). A series of AFM images is recorded in the contact-mode using triangular cantilevers with silicon nitride tips (tip radius <50 nm).

The crystal lattice structure of a pulverized UO_2 sample is analyzed by X-ray diffraction (Seifert XRD 3000, Ahrensburg, Germany). Electron backscatter diffraction (EBSD) of the altered UO_2 surface is performed in an environmental scanning electron microscope (Philips ESEM XL 30 FEG) equipped with a backscatter electron detector for imaging and a phosphorous screen/SIT camera to monitor Kikuchi patterns. As UO_2 is a semi-conducting sample, it can be analyzed by ESEM without a conducting surface coating which may impair backscatter diffraction bands. The electron beam in an ESEM penetrates several tenths to hundreds of nanometers into a sample bulk, depending on parameters like the accelerating voltage and material properties (i.e. densities). For the analysis of Kikuchi patterns the experimental arrangement is calibrated with respect to the working distance using a Ni standard. The calibration yields the position of the pattern centre on the screen, the specimen-to-screen distance and the specimen tilt. The grain orientations are obtained by comparison of the measured EBSD pattern with pattern calculated by the instrument software for the known crystal lattice. The general procedure of EBSD and orientation analysis is described in the literature [15,16].

3. Results

3.1. Morphological changes of the UO_2 surface during the dissolution process

Surface alterations can be imaged by electrochemical AFM under potentiostatic conditions at the surface nearly in real time. An overview of the UO_2 surface corroded by anodic oxidation is given in Fig. 2. Significantly different dissolution progress is observed at different grain faces, grain boundaries and etch pits, while simultaneously particulate deposits are formed.

For the determination of dissolution rates at constant potentials, a series of images is recorded with a time interval of about 5 min. The dissolution process is investigated under reducing and oxidizing conditions. Under strongly reducing condition (potential −1 V) no surface dissolution can be observed over a period one day which is the time frame of an in situ AFM experiment. Under strong oxidizing condition (+1 V) intense surface alteration is monitored over a period of about 3 h (Fig. 3). Height differences between a series of AFM images are quantified with reference to an area where the observed surface changes are small compared with the rest of the surface (the reference area is indicated with R in Fig. 3). This procedure represents a relative or semi-quantitative analysis of the dissolution progress, because absolute surface changes can only be obtained in the presence of unalterable reference points [17,18]. Fig. 3 shows a selected surface area of 11×11 μm^2 before and after a dissolution period of 103 min in 3% bicarbonate solutions ($NaHCO_3$).

The distinct changes in surface morphology are analyzed at a step between two grains (s), a grain boundary (gb) and at etch pits (p1, p2 and p3, see symbols in Fig. 3). The dissolution progress, i.e. height difference as a function of time, at these sample sites is plotted in Fig. 4. Dissolution rates can be calculated from the respective curve slopes (see insert in Fig. 4). Rates found at the step

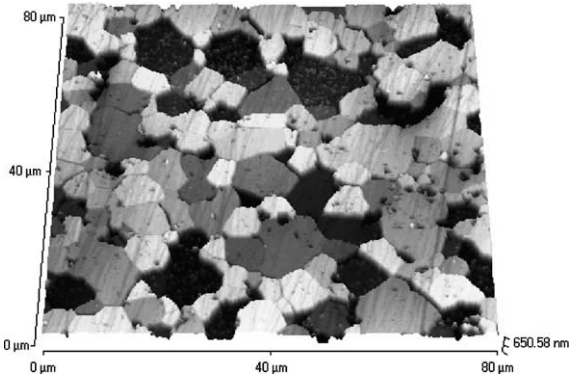

Fig. 2. AFM overview of a UO_2 surface after corrosion under oxidizing condition (reaction time 160 min; potential +1.0 V vs. Ag/AgCl; 3% sodium bicarbonate; pH = 8.7; see text).

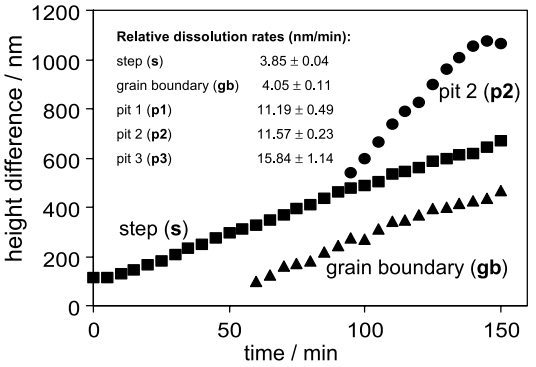

Fig. 4. Dissolution process at different sample sites as indicated in Fig. 3 (potential +1.0 V vs. Ag/AgCl; 3% sodium bicarbonate; pH = 8.7; see text).

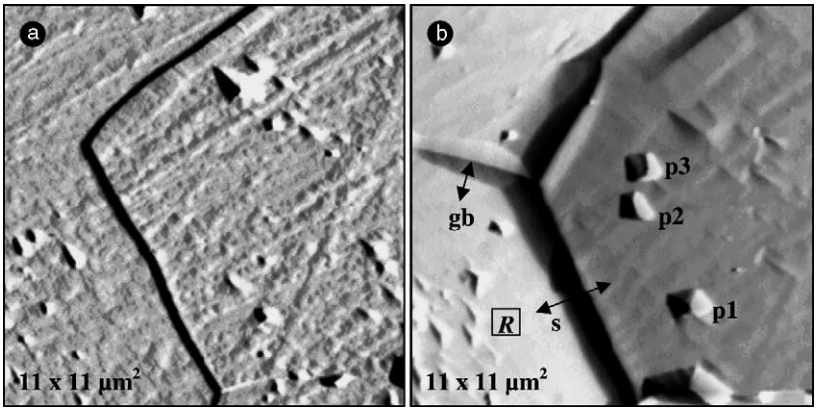

Fig. 3. UO_2 surface area before (a) and after (b) corrosion under oxidizing condition (reaction time 103 min; potential +1.0 V vs. Ag/AgCl; 3% sodium bicarbonate; pH = 8.7; symbols: grain boundary (gb), step (s), etch pits (p1, p2, p3), reference area (R); see text).

(s) between two grains and at the grain boundary (gb) provide similar values of 3.85 and 4.05 nm/min, respectively (see Section 4). The grain boundary (gb) exhibits a typical 'V' shape as illustrated schematically in [5]. At the etch pits (p1, p2, p3) threefold higher dissolution rates in the range of 11.1 and 15.8 nm/min are observed. This may be due to dislocations in the crystal or to local impurities.

3.2. Influence of redox potential and carbonate concentration on the dissolution rates

The dependence of the applied potential on the dissolution rate is investigated at two different concentrations of $NaHCO_3$ solution, 3% and 0.3%. A series of images is recorded for a period of about 30 min at a respective constant potential which is increased in steps of 100 mV from +100 to +600 mV (vs. Ag/AgCl). It is typical for AFM that images recorded over a longer period of time show a marked lateral drift, probably due to temperature fluctuations. This drift is corrected using a mathematical procedure described elsewhere [17,18].

Dissolution rates (in nm/min) at high carbonate concentrations (3%) are plotted against the applied potentials in Fig. 5. Three grains are selected in this plot with the highest rate observed, an intermediate and a low dissolution rate. For the selected grains the relationship between the applied potentials and the relative dissolution rates can be approximated by a linear function (see Section 4). From the curve fits for different grains a mean value of (0.03 ± 0.02) V can be calculated for the straight lines cutting the x-axis. This value can be regarded as a threshold for dissolution, because below this potential no dissolution is observed.

Similar investigations are performed in solutions with intermediate carbonate concentrations (0.3%) which are typical for natural aquatic systems. The results for 0.3% and 3% carbonate concentrations are compared for a grain face with a high dissolution rate in Fig. 6. As in the 3% carbonate solution, a linear relationship between the dissolution rates and the applied potentials is observed in 0.3% carbonate solution (see Section 4). From the curve fit, a value of (0.16 ± 0.03) V can be calculated as a threshold: no dissolution can be detected below this potential. Dissolution of UO_2 can be observed beyond this potential at rates which are 5–10 times smaller than in the 3% carbonate solutions. As described for the experiments in 3% carbonate, very different dissolution rates are found on different grain faces in 0.3% carbonate solution. Therefore, oxidative dissolution of the UO_2 surface is strongly enhanced by carbonate ions, which is in agreement with the literature (e.g. [1,2,19]). A dissolution mechanism is proposed in [2].

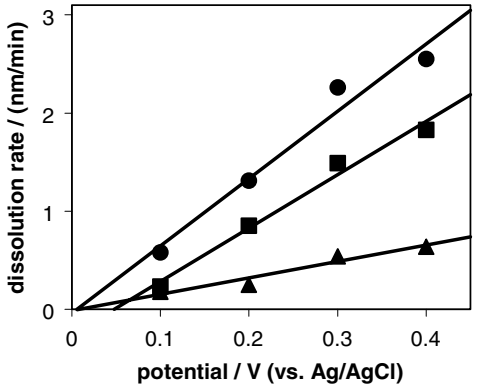

Fig. 5. Dissolution rates vs. redox potentials at three different grains with high (●), intermediate (■) and low (▲) dissolution rates (3% sodium bicarbonate; see text).

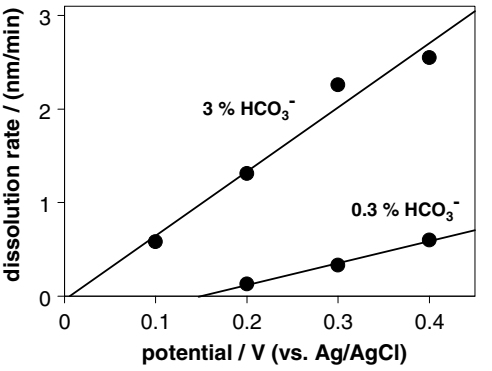

Fig. 6. Dissolution rates vs. redox potentials at grain faces with high dissolution rates (3% and 0.3% sodium bicarbonate; see text).

3.3. Remineralization

In addition to the electrochemical surface dissolution, particulate species are observed on grain faces with high dissolution rates, which can be seen in the overview of Fig. 2. These particles shown in Fig. 7(a) exhibit shapes of stacked platelets with irregular, partly angular contours, diameters and heights in the range of 200–900 and 10–150 nm, respectively. From AFM analysis alone one cannot decide whether these particles are crystalline or amorphous. Interestingly, the nucleation of these crystallites is not observed in the ECAFM dissolution experiments where the surface is continuously scanned by the AFM tip (see marked square in Fig. 7(b)). In this case, formation of small crystallites is probably disturbed by the movement of the AFM tip. On neighboring surface areas, which are not continuously scanned, a large number of platelet-shaped particles is found (outlying the square of Fig. 7(b)). These observations indicate that remineralization proceeds simultaneously at surface areas with high dissolution rates probably due to a local oversaturation of the solution

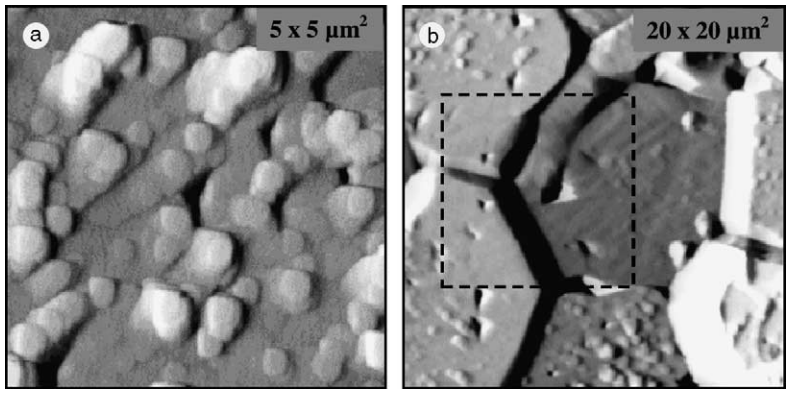

Fig. 7. (a) Remineralized particles formed on a UO_2 surface after corrosion under oxidizing condition; the marked square in (b) is the continuously scanned area of Fig. 3 (see text).

with uranyl carbonato ions and subsequent nucleation (see Section 4). The remineralized particles show a tabular morphology similar to that reported in [20].

3.4. X-ray diffraction (XRD) and electron backscatter diffraction (EBSD)

The crystal lattice structure of the UO_2 matrix is analyzed by X-ray diffraction (not shown). From a powder diffractogram a *face-centered* cubic structure (fcc) can be derived which is in agreement with the known fluorite structure of UO_2.

Different grains are investigated in an ESEM using a standard EBSD geometry. For a comparison of the measured Kikuchi pattern with the data base, the pattern centre, camera length and specimen tilt have to be calibrated as mentioned in Section 2. An ESEM image of the UO_2 surface with grains showing different dissolution progress and the related Kikuchi patterns are depicted in Fig. 8. Different grains with different dissolution progress exhibit different Kikuchi patterns and, as expected, different sites on the same grain form the same Kikuchi pattern (see numbers in Fig. 8). Therefore, different grains as fundamental building units of the material show different crystal orientations, whereas one grain apparently exhibits one predominant crystal orientation. No difference in the Kikuchi patterns could be detected when focusing the incident electron beam on the grain face or a remineralized platelet on top of it (see Fig. 8 and Section 4).

With the known fcc crystal lattice structure from XRD the number of possible and plausible patterns is

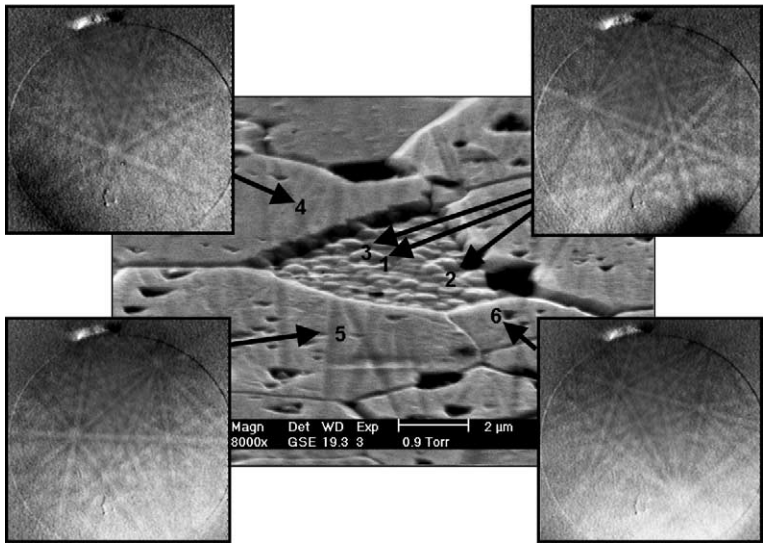

Fig. 8. ESEM image of a corroded UO_2 surface showing grains with different dissolution progress and the related Kikuchi patterns (see text).

strongly restricted. The software performs a Hough transformation, which extracts the dominant Kikuchi bands from the image. The width of the bands and their relative angles can be calculated. The orientation of the crystal atomic planes can be determined by comparison of the measured pattern with simulated or known pattern from a database. After this analysis, grains with the highest dissolution rates have a grain orientation with the (0 0 1) crystal plane parallel to the specimen surface. Grains with lower dissolution rates are characterized by *hkl* crystal planes of higher order parallel to the sample surface. Therefore, the grain orientation is found to play a major role in the inhomogeneous dissolution of UO_2 pellet surfaces.

4. Discussion

In this study UO_2 surface alterations are directly investigated at the solid–water interface applying different redox potentials. Dissolution rates increase with increasing oxidizing potentials and with carbonate concentration which is in general agreement with results from previous studies [1,2]. The reasons for this behaviour are the increased solubility of U(VI) compared to U(IV) and the carbonate complexation of UO_2^{2+} ions. The observed linear relationship between the corrosion potential and the corrosion rate differs from that described in the literature, where a linear relationship between the corrosion potential and the logarithm of the corrosion rate is reported (e.g. [1,5]). In the literature experiments steady-state conditions are aspired using flow-through cells or rotating disc electrodes in order to avoid unwanted surface reactions [1,22]. The presented ECAFM experiment is performed without flow-through or stirring and, therefore, far away from steady-state. A local near-surface oversaturation with uranium carbonato ions during dissolution and the subsequent formation of surface intermediates on the UO_2 electrode (Fig. 7) probably limits the measured dissolution rates. It can be assumed that these processes determine the observed quasi-linear relationship between potential and corrosion rate (Figs. 5 and 6) and lead to reduced curve slopes especially at higher potentials ($\geqslant 0.3$ V). These results provide further evidence to the presumed influence of surface intermediates on the corrosion process as described in the literature (e.g. [5,19]). The non-steady-state condition seems also to be responsible for the observed dissolution threshold in the 0.3% carbonate solution (Fig. 6). In carbonate-free solutions, surface dissolution is blocked by the formation of oxidized secondary phases, whereas available carbonate near the surface enhances the solubility by formation of uranyl carbonates [19]. In the 3% carbonate solution, dissolution starts with positive oxidizing potential, which is in agreement with the literature (e.g. [1,19]). In the 0.3% carbonate solution, the limited availability of carbonate near the surface seems to restrict the dissolution process until a certain oxidizing potential is reached. This interpretation is in agreement with strongly reduced dissolution currents under non-steady-state conditions and the control of the dissolution process by carbonate as reported in the literature (e.g. [1,2,19]).

It is shown that the dissolution rate strongly depends on the grain orientation, where the (0 0 1) crystal plane parallel to the surface exhibits the highest dissolution rate. Enhanced dissolution rates are also observed at several grain boundaries exhibiting a typical 'V' shape (Figs. 2 and 3). An explanation from the literature is the degree of non-stoichiometry in the grain boundaries (UO_{2+x}) enhancing the uranium oxide conductivity. In the present study, similar dissolution rates of fast dissolving grain faces and grain boundaries are determined (Figs. 3 and 4). From this observation one may speculate that fast dissolving grain boundaries are again the borders of fast dissolving grain faces with the (0 0 1) crystal plane orientated perpendicular to the surface. This assumption is supported by the observation that grain boundaries do not generally dissolve faster than the neighboring grain faces. In Fig. 2, one can find as well grain boundaries exhibiting slow dissolution rates similar to that found at neighboring grain faces. Therefore, special effects at grain boundaries originating from non-stoichiometry or impurities probably influence but do not dominate the dissolution rates under these experimental conditions.

Particulate species with tabular morphology are formed during the corrosion predominantly on grain faces with high dissolution rates probably due to a local oversaturation with uranyl carbonato ions. The nucleation of these crystallites may occur on edge pits (as reactive sites) which are formed in consequence of dissolution (Fig. 3(b)). The Kikuchi patterns of the deposited particles and the underlying grain face cannot be differentiated. This is not due to the information depth of backscattered electrons which can be estimated to be <20 nm and, therefore, is in the range of measured particle heights (see [21] for the definition and estimation of the information depth). A possible reason for the insensitivity to surface particles is the geometry of the EBSD experimental setup, where the angle between the incident electron beam and the sample surface is adjusted to approximately 20°. Due to the penetration depth of the incident electrons, the backscattered electrons may escape from a sample site which is distinctly displaced from the focused particle. Therefore, backscatter Kikuchi bands apparently measured in a deposited particle may originate from the underlying crystal face. Furthermore, it is not evident if the surface deposits provide a crystalline structure which is essential for the formation of backscatter Kikuchi bands. Further

EBSD measurements have to be performed to clarify these questions.

5. Conclusions

The combined ECAFM and EBSD results indicate that the dissolution kinetics of polycrystalline UO_2 is strongly influenced by the grain orientations. The subsequent increase of the pellet surface may accelerate the macroscopically observed dissolution rates. Furthermore, the preferred dissolution of grains and the occurrence of etch pits may result in a collapse of the fuel pellet. On the other hand, the local formation of secondary phases by near-surface oversaturation of the solution with U(VI) may act in the opposite direction. The identification of the deposited secondary phases will help to understand the mechanism of remineralization in order to estimate the actinide release. As discussed in the literature, UO_2 dissolution rates strongly depend on the applied experimental conditions such as pH, carbonate concentration, redox and flow conditions (e.g. [22]). The presented electrochemical setup allows the control of the redox conditions at the UO_2 surface which is essential for a comparison of dissolution rates obtained by different experimental approaches. By the combination of a microscopic technique with an electrochemical setup in ECAFM only very small sample sizes are needed which may be in particular advantageous for the study of spent fuel surface chemistry.

References

[1] D.W. Shoesmith, J. Nucl. Mater. 282 (2000) 1.
[2] J. de Pablo, I. Casas, J. Gimenez, M. Molera, M. Rovira, L. Duro, J. Bruno, Geochim. Cosmochim. Acta 63 (1999) 3097.
[3] D.W. Shoesmith, S. Sunder, Svensk Kärnbränslehantering AB, Swedish Nuclear Fuel and WasteManagment, SKB Technical Report 91-63, 1991.
[4] E. Smailos, Nucl. Technol. 104 (1993) 343.
[5] D.W. Shoesmith, W.H. Hocking, B.M. Ikeda, F. King, J.J. Noel, S. Sunder, Can. J. Chem. 75 (1997) 1566.
[6] Electrochemical techniques applied to natural UO_2 corrosion in aqueous solutions, in: Institute for Transuranium Elements, Annual Report 1992, EUR 15154 EN, p. 93.
[7] U. Kamachi Mudali, Y. Katada, Electrochim. Acta 46 (2001) 3735.
[8] R.E. Williford, C.F. Windisch Jr., R.H. Jones, Mater. Sci. Eng. A 288 (2000) 54.
[9] G. Bertrand, E. Rocca, C. Savall, C. Rapin, J.-C. Labrune, P. Steinmetz, J. Electroanal. Chem. 489 (2000) 38.
[10] J.P. Bearinger, C.A. Orme, J.L. Gilbert, Surf. Sci. 491 (2001) 370.
[11] C. Muggelberg, M.R. Castell, G.A.D. Briggs, D.T. Goddard, Surf. Sci. 402–404 (1998) 673.
[12] R.A. Schwarzer, Micron 28 (1997) 249.
[13] A.J. Schwartz, M. Kumar, B.L. Adams (Eds.), Electron Backscatter Diffraction in Material Science, Kluwer Academic/Plenum, New York, 2000.
[14] R. Holze, Leitfaden der Elektrochemie, B.G. Teubner, Stuttgart, Leipzig, 1998.
[15] A.J. Wilkinson, P.B. Hirsch, Micron 28 (1997) 279.
[16] B.L. Adams, S.I. Wright, K. Kunze, Metall. Trans. 24A (1993) 819.
[17] M. Plaschke, J. Römer, J.I. Kim, Ultramicroscopy 75 (1998) 77.
[18] J. Römer, M. Plaschke, J.I. Kim, Ultramicroscopy 85 (2000) 99.
[19] D.W. Shoesmith, S. Sunder, T.C. Tait, J. Nucl. Mater. 257 (1998) 89.
[20] M.E. Torrero, I. Casas, J. de Pablo, M.C.A. Sandino, B. Grambow, Radiochim. Acta 66&67 (1994) 29.
[21] M.P. Seah, W.A. Dench, Surf. Interf. Anal. 1 (1979) 2.
[22] S. Röllin, K. Spahiu, U.-B. Eklund, J. Nucl. Mater. 297 (2001) 231.